

16

Unraveling East Africa's Climate Paradox

Bradfield Lyon¹ and Nicolas Vigaud²

ABSTRACT

An observed drying trend and projected increase in rainfall place East Africa in an apparent climate paradox. It is argued that the observational evidence, backed by climate modeling experiments, support the case that the recent regional scale drying trend in East Africa was dominated by an abrupt decline in March–May rainfall around 1998–1999 and associated with a shift of Pacific decadal variability (PDV) to its cold phase. While it is possible a warming trend in the western tropical Pacific contributed to the severity of recent droughts, the timing of the recent decline is closely tied to PDV. Thus, the paradox is seen to result from a mismatch of timescales on one hand (recent drying versus long-term wetting) and from taking climate change projections at face value on the other. The inability of coupled models to capture fundamental aspects of the current climate undermines confidence in the future climate projections in East Africa. Given substantial errors in coupled climate models' ability to simulate the current climate, it remains an open question as to whether or not the future climate in East Africa will become wetter as a result of anthropogenic climate change.

16.1. INTRODUCTION

Several East African countries are currently facing something of a climate paradox [Lyon, 2014]. For well over a decade, the region has been experiencing an increased frequency of drought (Fig. 16.1a), the most recent and severe of these events (in 2010–2011) triggering a humanitarian crisis and prompting a major international response [FEWSNET, 2011]. This rainfall decline has led to inevitable speculation that an anthropogenic climate change signal has begun to emerge in the region. Yet, paradoxically, climate model projections show a general consensus that increasing greenhouse gasses will in fact result in East Africa's climate becoming *wetter* during the cur-

rent century (Fig. 16.1b) [Christensen *et al.*, 2007; Shongwe *et al.*, 2011]. Confounding this seeming paradox, in many parts of East Africa the rainfall seasonal cycle is bimodal, with the bulk of the recent rainfall decline occurring during the “long rains” season of March–May (MAM; other seasons denoted similarly) while the “short rains” of October–December (OND) show an upward trend over the past three decades [e.g., Liebmann *et al.*, 2014].

These divergent outcomes highlight the need to identify the physical mechanisms associated with both the observed and projected changes in East African climate. From a physical perspective, a true paradox is of course illusory and several hypotheses can be contemplated to account for the differing trends. For example, the coupled climate models (CMIP5) used to project the future climate may be missing, or misrepresenting, key physical processes important to East African rainfall. The future may indeed become drier and the model projections are simply wrong. Alternatively, the recent drying may be a

¹*School of Earth and Climate Sciences and Climate Change Institute, University of Maine, Orono, Maine, USA*

²*International Research Institute for Climate and Society, The Earth Institute, Columbia University, Palisades, New York, USA*

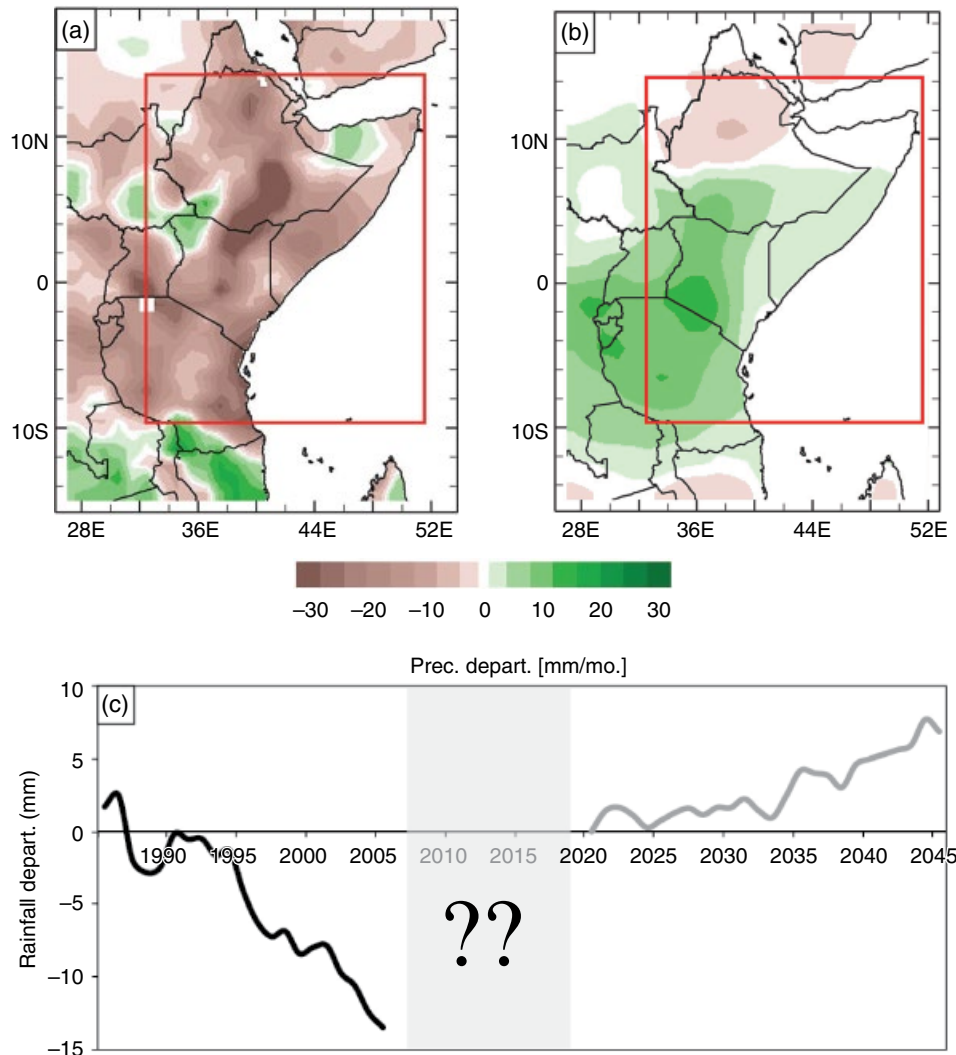


Figure 16.1 (a) Difference in MAM rainfall (mm/mo) between the periods 1999–2010 and 1977–1998. (b) Multimodel mean CMIP5 change in MAM rainfall for 2035–2050 minus 1970–2000. (c) 9 year moving averages of MAM rainfall anomalies for East Africa (boxed region) in observations (GPCC, black line) and in the multimodel mean of CMIP5 projections (grey line), the latter arbitrarily set to zero in 2020.

manifestation of lower-frequency natural climate variability, with the longer-term response to increasing greenhouse gases leading to more rainfall. A third hypothesis is that natural climate variations and anthropogenic climate change already underway may have constructively interfered, the latter increasing the severity of recent rainfall anomalies in East Africa while the future remains uncertain. Other hypotheses can of course be envisioned.

This chapter attempts to unravel some aspects of the apparent East African climate paradox by focusing primarily on the recent rainfall decline. The role of Pacific decadal variability will be discussed along with its possible interaction with long-term trends in sea surface temperatures (SSTs), particularly in the western equatorial

Pacific. Some important errors in CMIP5 model simulations of the current East African climate will be detailed, which have substantial implications for interpreting future climate changes in the region. While these topics fall squarely within the realm of climate science, it is stressed that an increased understanding of East African climate variability and change has substantial ramifications outside of that sphere. East Africa is one of the most food-insecure areas of the world [FAO *et al.*, 2014]. The severe drought of 2010–2011 in Kenya, Somalia, and southeastern Ethiopia, for example, affected some 10 million people and was a contributing factor to more than 250,000 fatalities in Somalia alone [UN OCHA, 2011; Checchi and Robinson, 2013]. The hope is that an improved scientific understanding of East African climate

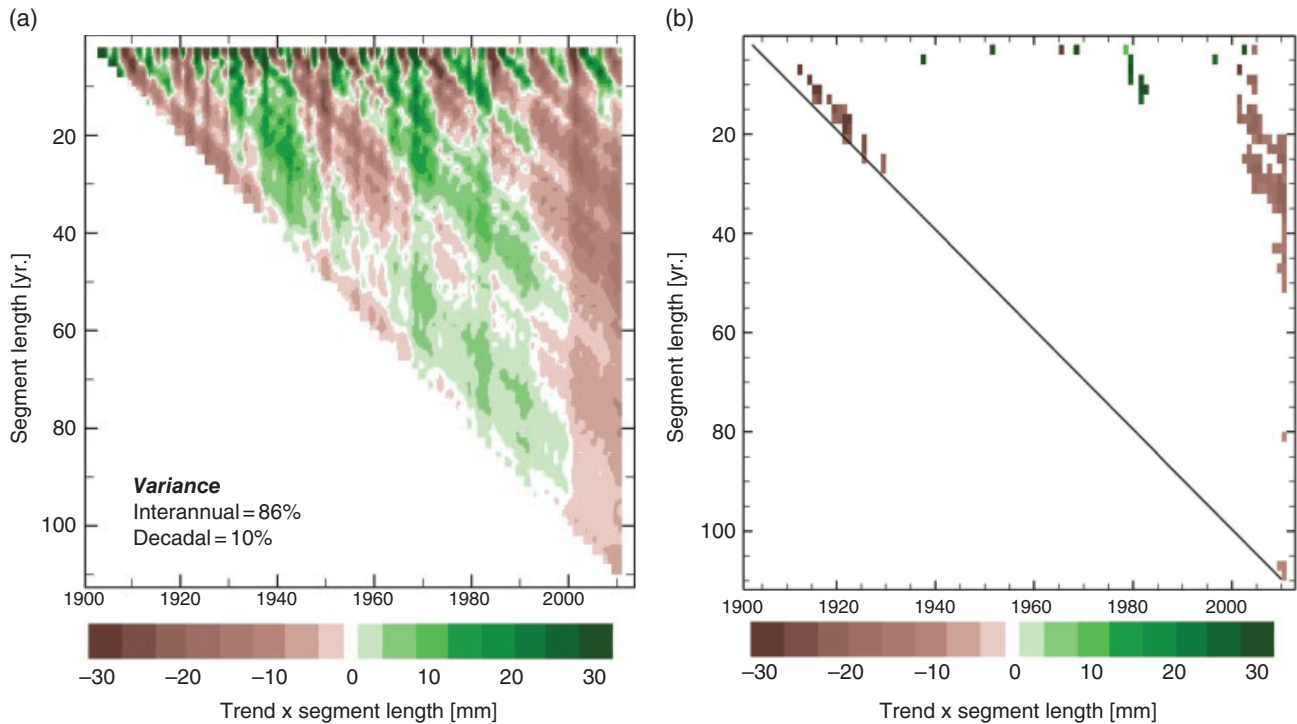


Figure 16.2 (a) Linear trend multiplied by segment length over which it was computed (shading, mm) for the East African MAM long rains in GPCC. Vertical axis is segment length, horizontal axis is the end date of fitted trend. The percent of variance for interannual and decadal scale fluctuations is shown at the lower left. (b) Statistically significant values ($p < 0.05$) based on a two-tailed t test. Adapted from Lyon [2014]. (See insert for color representation of the figure.)

will ultimately translate into better preparedness in order to mitigate impacts from the climate extreme of drought.

16.2. THE NATURE OF THE RECENT EAST AFRICAN LONG RAINS DECLINE

16.2.1. Evidence of an Abrupt Shift in Regional MAM Rainfall

Secular trends in climate data time series are ubiquitous as the climate system is continuously varying on multiple timescales. An illustration of this behavior for East African MAM seasonal rainfall is provided in Figure 16.2, which displays linear trends in precipitation averaged over the boxed region in Figure 16.1 (land areas only) as a function of (varying) segment length and end date. The underlying data are from the Global Precipitation Climatology Center (GPCC) version 6 [Schneider *et al.*, 2008] and the methodology follows that of Liebmann *et al.* [2010]. Large interannual variations in rainfall clearly affect short-term trends (e.g., segments < 10 years) in Figure 16.2, with decadal to multi-decadal fluctuations also evident on longer timescales. In terms of rainfall variance (1901–2010), MAM rainfall is

dominated by interannual fluctuations (86% of total variance) while decadal variations (based on a 9 year moving average) account for 10%. Of particular interest are the negative trends for segment lengths $> \approx 10$ years starting around the year 2000. Statistically significant ($P < 0.05$) downward trends for time segments of around 15–30 years occur after that time (Fig. 16.2b). The abruptness of these changes suggests a rapid transition to very dry MAM seasons in recent years.

Evidence for an abrupt decline in MAM rainfall in East Africa is revealed in several different datasets. Since the number of stations in the GPCC dataset varies with time and may affect the analysis, outgoing longwave radiation (OLR) was also used here as a proxy for rainfall, the latter also having the desirable attribute of being a completely independent dataset. (Note, outgoing longwave radiation data are from the US Climate Prediction Center and downloaded via the International Research Institute for Climate and Society [IRI] Data Library at <http://iridl.ldeo.columbia.edu/SOURCES/.NOAA/.NCEP/.CPC/.GLOBAL/.monthly/.olr>.)

Results for both variables are shown in Figure 16.3, the top panel first showing the difference in monthly rainfall averaged across East Africa (boxed region in Fig. 16.1)

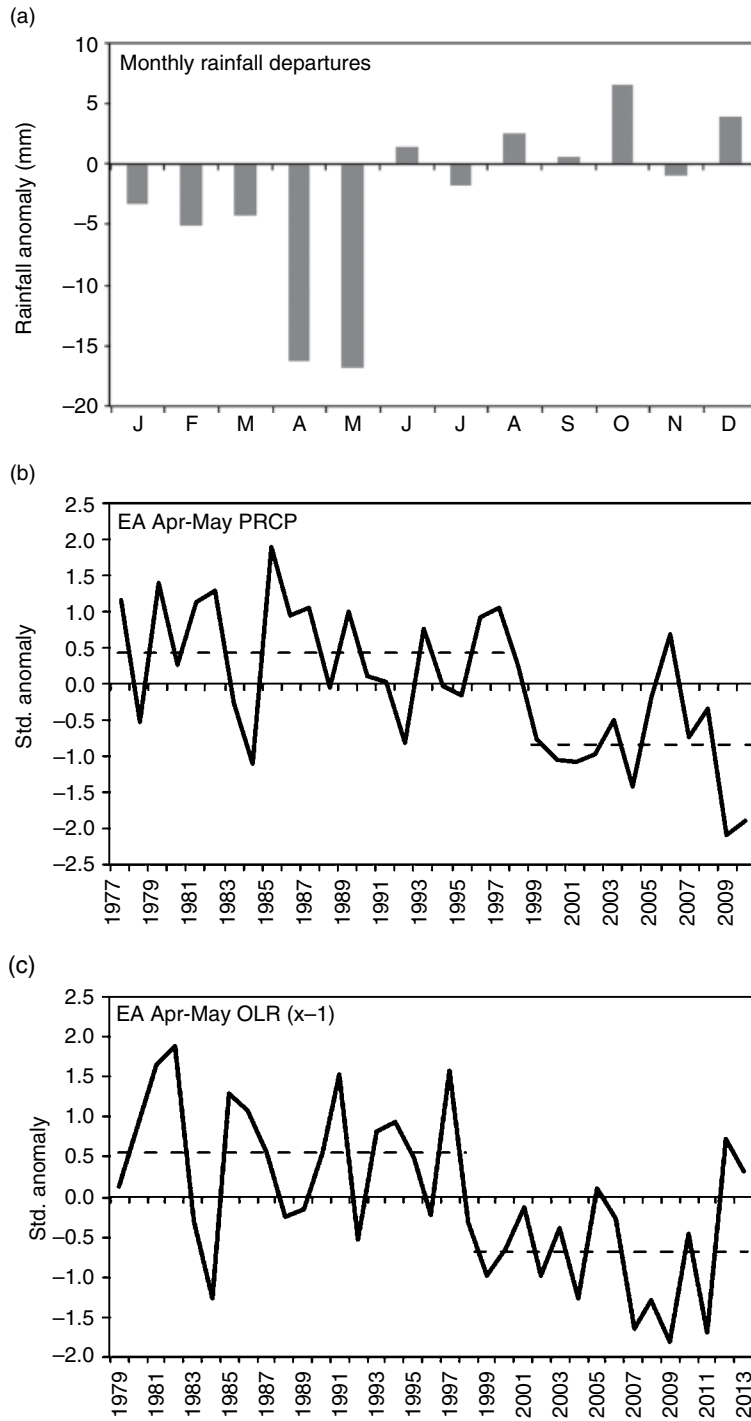


Figure 16.3 (a) Monthly rainfall differences for East Africa (mm) between the periods 1999–2013 and 1977–1998. (b) April–May season standardized rainfall departures from a 1977–2010 mean. Dashed horizontal lines indicate mean values for two epochs before and after a change point in 1999. (c) As in (b), but for OLR anomalies (x -1). The most likely shift in (c) occurs in 1998.

between the periods 1999–2010 and 1977–1998 (using GPCP data). April and May are seen to have the greatest negative departures while the OND season, on average, exhibits relative *wetening* during the most recent period. Why were these two specific periods chosen? Figure 16.3b

and c show time series of standardized MAM rainfall and OLR anomalies (multiplied by -1) averaged across East Africa (land areas only) for past three-plus decades. Apparent shifts in both these series occur around 1998–1999. As an objective means of identifying such potential

change points, the RHtestV4 software package [Wang, 2008] was used. While this and related tools are typically used to identify nonclimate (and thus, spurious) break points in time series, here it is used to identify likely shifts that will be related to decadal variations in the climate system. Using this tool, a statistically significant change point ($p < 0.05$) was identified in GPCC rainfall, most likely occurring in 1999. The OLR data also exhibit a statistically significant shift ($p < 0.01$), most likely occurring in 1998. The linear correlation between the OLR and GPCC time series is $r = 0.8$ indicating the latter is able to capture a significant portion of the GPCC rainfall variance in addition to a near-synchronous shift in mean behavior. As mentioned, these shifts are argued to reflect physical changes in the climate system, with evidence for their association with Pacific decadal variability (PDV) summarized in section 16.3. The time series in Figure 16.3 provides a cautionary note when interpreting trends in temporally smoothed time series: the average across a “step” yields a “ramp,” which can be misinterpreted as a longer-term trend rather than a more abrupt change.

16.2.2. Recent Changes in the Seasonality of the MAM Long Rains

Changes in the seasonal cycle of the long rains were examined using the Climate Hazards Group InfraRed Precipitation with Station data (CHIRPS) gridded daily rainfall dataset [Funk *et al.*, 2014]. The CHIRPS rainfall data are based on satellite estimates combined with in situ station data to provide some calibration. The data used were on a 0.25° lat. \times lon. grid and covered the period 1981–2014. As a first step, a 1981–2010 base period monthly climatology was generated and used to identify grid points in the East African domain where the climatological mean MAM rainfall was less than 25% of the mean annual total (indicating a relative dry season). Such dry season locations (representing 23% of land area grid points) were dropped before undertaking subsequent computations. Figure 16.4a shows the accumulated, mean daily rainfall from 1 March to 31 May averaged over the periods 1981–1998 and 1999–2014 and for the seven driest MAM seasons during the post-1998 period identified in the CHIRPS data (2000, 2001, 2004, 2007, 2008, 2009, 2011). The figure indicates the expected lower rainfall accumulations for the post-1998 period, but differences in accumulations from the earlier period do not emerge until April, generally consistent with the results in Figure 16.3a, which was based on a different dataset (and where there was no masking for seasonality). For the seven driest MAM seasons in the post-1998 period, relative deficits emerge earlier, during the month of March.

Further changes in the seasonal cycle of the East African long rains are shown in Figure 16.4b, which

displays average daily rainfall differences from a February to June mean value (using a 1981–1998 base period). A 15 day running average has been applied to smooth all three series shown in the figure. Using a zero threshold crossing as a simple benchmark for the regional onset of the long rains, this crossing is seen to occur in mid-March during both the 1981–1998 and 1999–2014 periods. Thus, by this definition, there is no systematic shift identified in the onset date of the long rains during the post-1998 period. What is seen, however, is an earlier cessation of the long rains during recent years. This is consistent with an earlier onset of the Indian summer monsoon [e.g., *Camberlin et al.*, 2010; *Kajikawa et al.*, 2012]. For the seven driest years in the post-1998 period, Figure 16.4b shows both a delayed onset and early demise of the long rains. *Camberlin and Okoola* [2003] found that a shorter rainy season is generally associated with reduced total seasonal rainfall, which was certainly the case in these recent drought years.

Overall, there is observational evidence from independent datasets that the recent decline in MAM rainfall in East Africa was associated with an abrupt downward shift around 1998–1999. Subseasonal changes in MAM are noted as well, most notably an earlier cessation of the rainy season (on the regional scale), which during the worst of the recent drought years was also accompanied by a delayed onset. The greatest contribution to the seasonal decline was a marked decrease in rainfall during the months of April and May. While abrupt and statistically significant shifts in East African rainfall and OLR are identified, this begs the question of an underlying cause. Their linkage to PDV is discussed in the next section.

16.3. LINKS TO PACIFIC DECADAL VARIABILITY

Supporting evidence that the abrupt shift in the East African long rains was associated with PDV is provided in Figure 16.5, which shows time series of detrended MAM rainfall anomalies (from GPCC) averaged over East African land areas (boxed region in Fig. 16.1) and the principal component time series of the leading mode of SST variations in the Pacific Ocean after removing the long-term trend and instantaneous influence of the El Niño–Southern Oscillation [from *Lyon*, 2014]. The latter SST index is significantly correlated ($r = 0.7$, $p < 0.05$) with the Pacific Decadal Oscillation (PDO) index of *Mantua et al.* [1997], with both indicating nearly synchronous phase shifts, including a shift to the cold phase in 1998–1999. Both time series in Figure 16.5 have been smoothed with a 9 year moving average and cover the period 1905–2005. Coherent temporal variations between these variables are seen across the full analysis period, the temporal correlation being $r = 0.72$, which is statistically significant at $p < 0.01$ based on a two-tailed t-test.

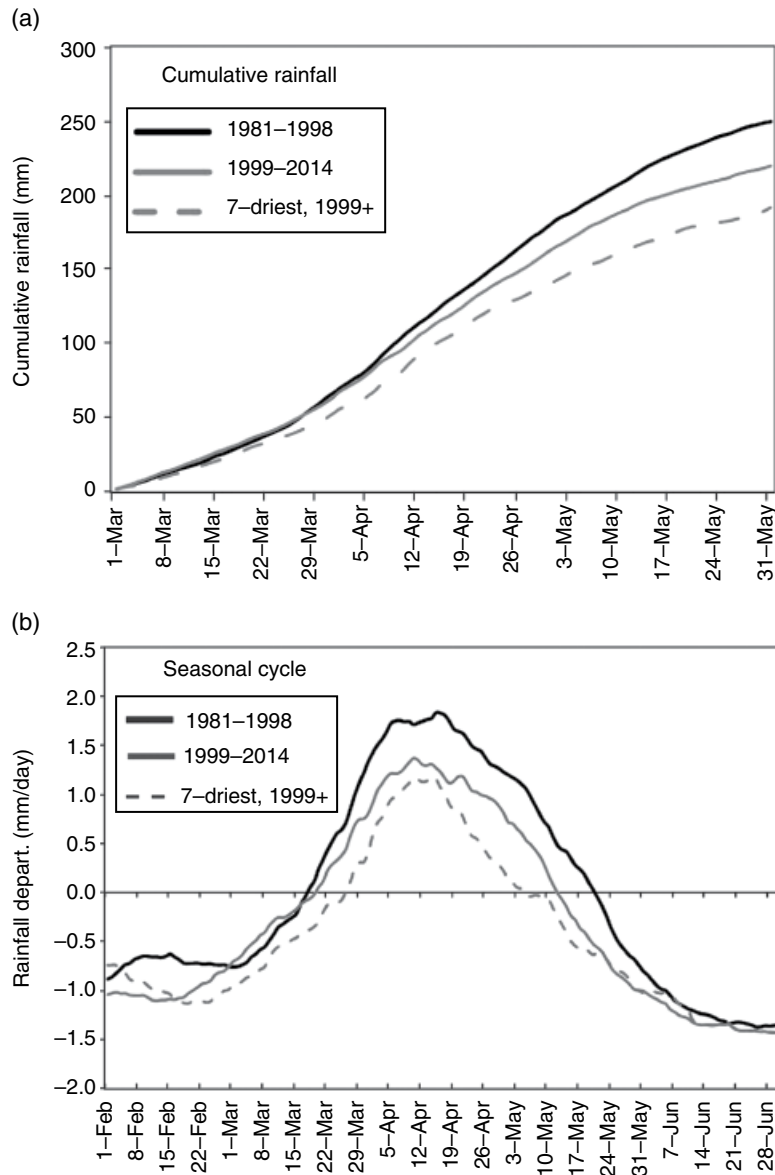


Figure 16.4 (a) Average, cumulative daily rainfall (mm) across East Africa land locations for 1 March–31 May based on CHIRPS data. Solid black (grey) line is the average for the period 1981–1998 (1999–2014) and dashed line for the seven driest MAM seasons during the post-1998 period. (b) Daily rainfall departures (mm/day) from a 1981–1998 average of 1 February–30 June area-average rainfall in CHIRPS for the periods 1981–1998 (solid black line), 1999–2014 (solid grey line) and the seven driest MAM seasons in the post-1998 period (dashed grey line).

Building on the above result, Figure 16.6 displays differences in average MAM precipitation (from GPCC) between the cold phases of PDV that have occurred over roughly the past 100 years and its most recent warm phase, during 1977–1998 [after Lyon, 2014]. The rainfall anomaly patterns are remarkably similar for all three periods, not just in Eastern Africa, but also across many other land areas of the globe. While there are certainly concerns regarding the quality of the GPCC data going back to the start of the twentieth century, it is exceedingly

unlikely that the similar rainfall anomaly patterns in Figure 16.6 occurred by chance. The pattern correlation (55°S – 55°N), for example, between rainfall anomalies for the periods 1999–2010 and 1914–1925 is $r=0.53$. Assuming (quite conservatively) 25 spatial degrees of freedom in MAM rainfall for this domain [e.g., Van den Dool and Chervin, 1986] the probability of a chance occurrence is $p < 0.01$ based on a two-tailed t-test.

Additional evidence for abrupt changes in the climate system around 1998–1999 is provided in Figure 16.7,

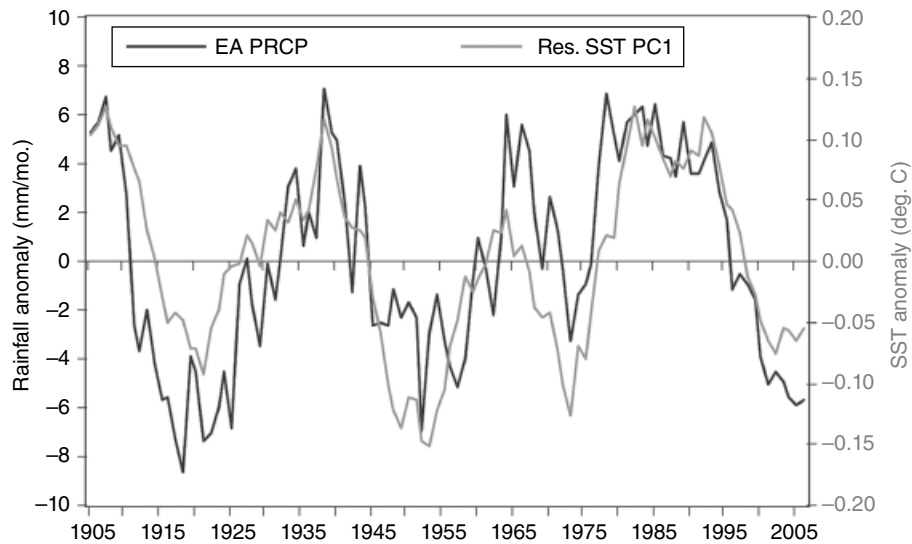


Figure 16.5 Time series of the leading PC ($^{\circ}\text{C}$, right scale) from the residual SST EOF analysis from ERSST (multiplied by -1 , gray line) and the detrended East African rainfall anomaly (mm/mo, left scale) for MAM. A 9 year moving average has been applied to both series. The temporal correlation between the series is $r = 0.73$ over the full 102 year period (1905–2006). Adapted from Lyon [2014]. See electronic version for color representation.

the top panel showing differences in SST between MAM seasons averaged over 1999–2014 and 1977–1998. These differences have been divided by the standard deviation of MAM SST anomalies (1981–2000) and are expressed in dimensionless, standardized units. East of the dateline, the tropical Pacific has cooled with anomalies exceeding minus one standard deviation in the eastern portion of the basin. Conversely, the western Pacific exhibits substantial positive SST anomalies, exceeding 1.5 standard deviations southeast of the Philippines and north of the equator (SSTs in this region also exhibit a substantial upward trend, which will be discussed further in section 16.4). Standardized SST differences are generally positive but of much smaller magnitude over the Indian Ocean.

Time series of anomalous (1979–1998 base period) MAM SST and rainfall averaged over the Pacific warm pool region (boxed area in Fig. 16.7a) are plotted in Figures 16.7b and c, respectively. The SST time series indicates an upward trend although there is considerably less variance in the series for the post-1998 period. MAM rainfall anomalies (from GPCPv2.2, Huffman *et al.* [2009], and CMAP, Xie and Arkin [1997]) over this region exhibit substantially different behavior than SST, with an abrupt upward shift in 1999, identified as a statistically significant ($p < 0.05$) change point in both datasets. Increased rainfall in the Pacific warm pool region has been associated with an intensification of the overturning Walker circulation across the Indian Ocean, with its descending branch favoring decreased rainfall over East Africa [Funk *et al.*, 2013; Hoell *et al.*, 2014; Liebmann

et al., 2014]. Chapter 4 of this book also discusses the western Pacific warming effect.

The above results suggest that a sustained intensification of the ascending branch of the Walker circulation occurred only after 1998, which coincides with the shift in PDV to its cold phase. By contrast, the warming of the Pacific warm pool has been fairly continuous over the past four decades and would thus not appear to be able to account for this abrupt behavior. The warming may have served to increase the *intensity* of the Walker circulation (and thus drying over East Africa) but it cannot by itself account for the *timing* of the transition. This will be discussed further in the next section.

16.4. PHYSICAL CONSIDERATIONS

As mentioned, a dynamical link between Pacific warm pool rainfall and drying in East Africa is an enhanced overturning Walker circulation [Hoell and Funk, 2013, 2014; Hoell *et al.*, 2014; Liebmann *et al.*, 2014], which is consistent with other studies [Lyon and DeWitt, 2012; Lyon *et al.*, 2014; Yang *et al.*, 2014]. Figure 16.8 shows the midtropospheric pressure vertical velocity for MAM along with the magnitude of the zonal wind component at 850 and 250 hPa as seen in the European Centre for Medium Range Weather Forecasts reanalysis (ERA-Interim, Dee *et al.* [2011]; negative values indicating *upward* motion). Values in the figure represent averages from 10°S to 10°N and are expressed as the difference between the periods 1999–2013 and 1979–1998. Enhanced upward motion is identified over the western tropical

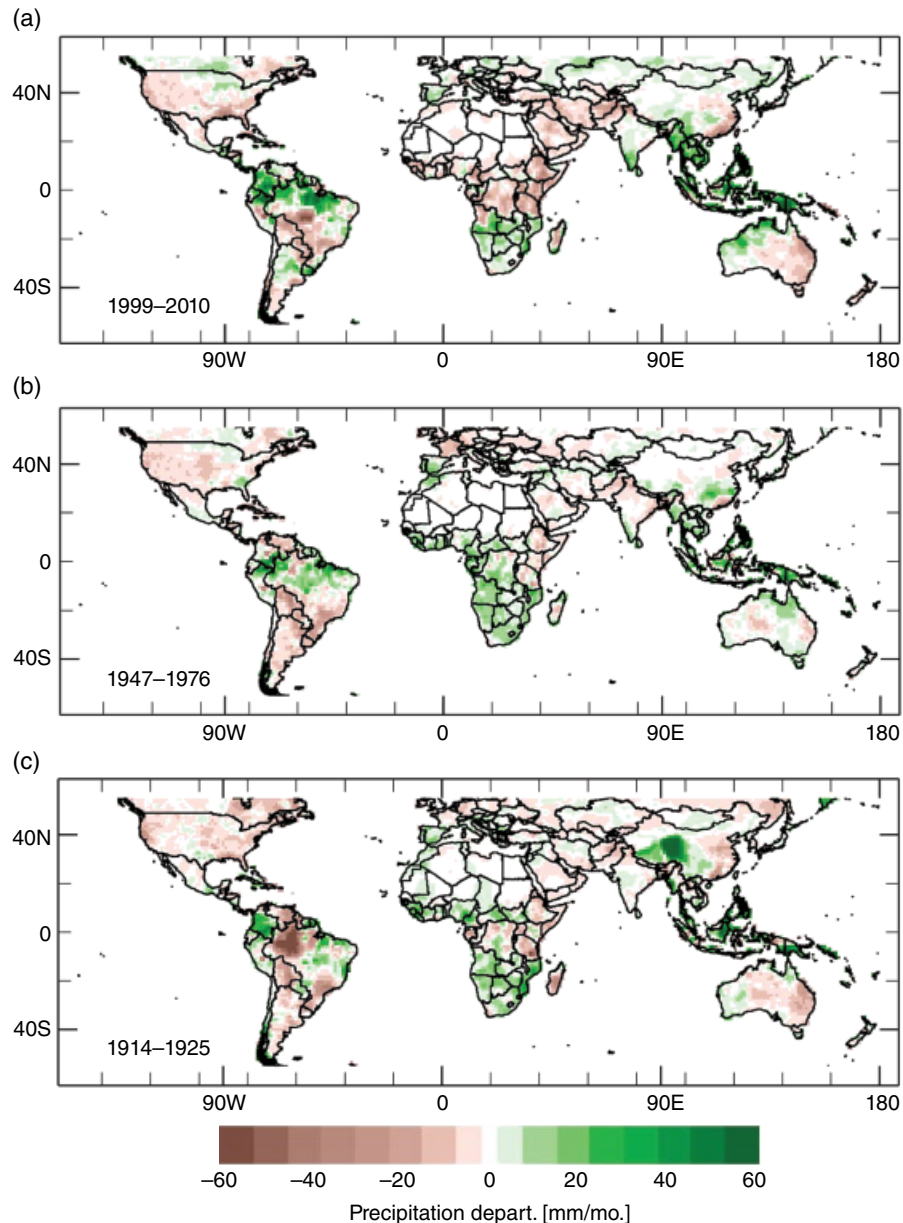


Figure 16.6 MAM precipitation differences (mm/mo.) between averages for (a) 1999–2010, (b) 1947–1976, and (c) 1914–1925 with the average for 1977–1998. Adapted from *Lyon* [2014].

Pacific centered near 135°E (the Pacific warm pool region), while enhanced descent relative to 1979–1998 is identified across most of the equatorial Indian Ocean to the west and the east-central Pacific to the east. The anomalous winds are also consistent with enhanced Walker cells. In the horizontal plane, the increase in rainfall in the Pacific warm pool region north of the equator (Fig. 16.7c) is consistent with previously identified anomalous 850hPa westerlies across the northern Indian Ocean during the post-1998 period [*Lyon and DeWitt, 2012; Lyon et al., 2014*]. Such an asymmetric (relative to the equator) wind pattern across the Indian Ocean is an

expected Gill-type response to an off-equatorial heat source located farther east. This wind pattern is also consistent with an earlier cessation of the MAM long rains season since 1998, as increasingly divergent flow over East Africa becomes established earlier than occurs climatologically [*Yang et al., 2015*].

While the recent and abrupt decline in East African rainfall exhibits linkages to PDV, this does not exempt a possible contribution from anthropogenic forcing. As mentioned, an upward trend in west Pacific warm pool SSTs has been observed over the past several decades. These higher SSTs have been associated with an increase

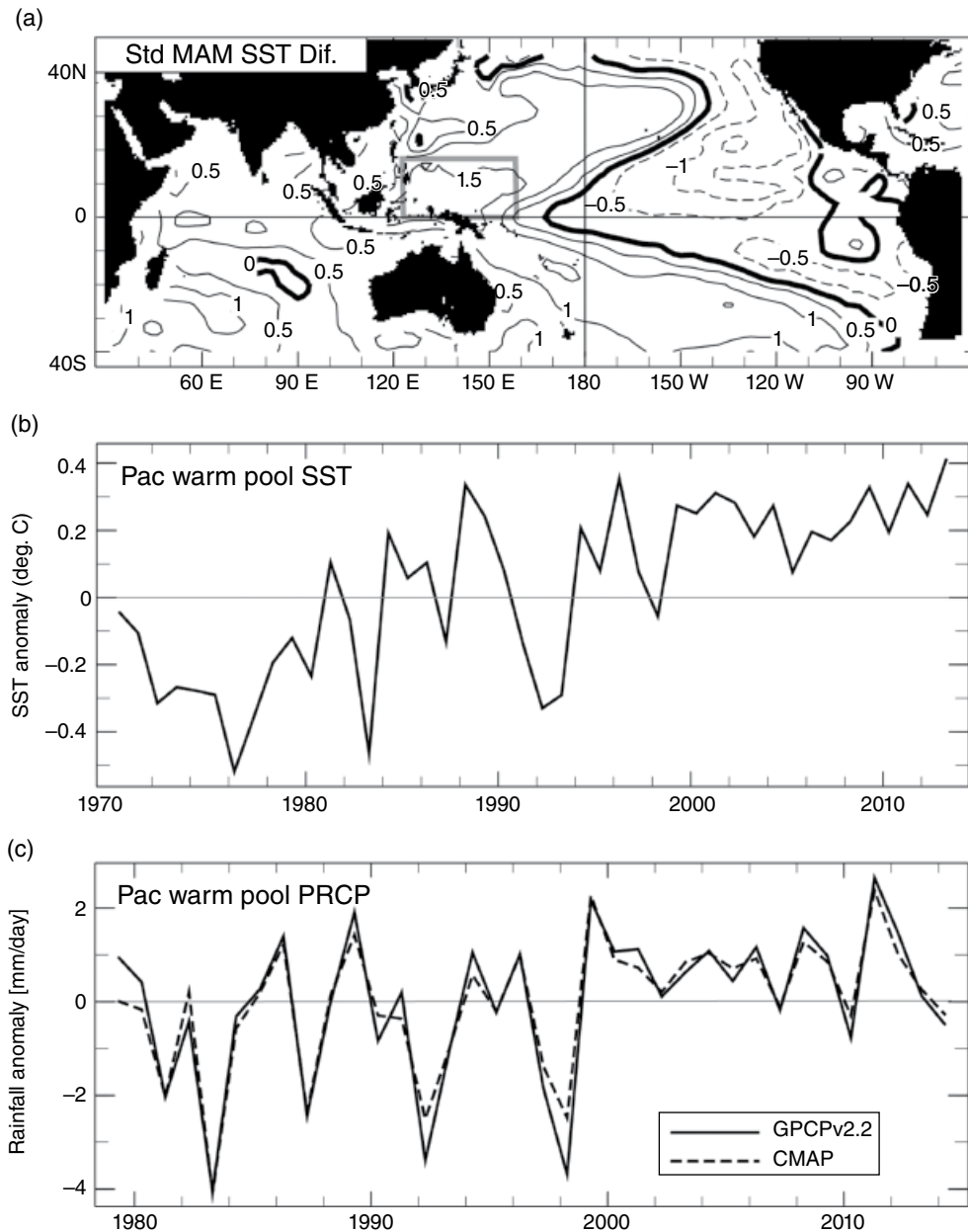


Figure 16.7 (a) Standardized difference in MAM SST between the periods 1999–2014 and 1977–1998 (dimensionless). (b) Time series (1970–2014) of MAM SST anomalies (deg. C) in the Pacific warm pool region (boxed region in [a]). (c) As in (b), but for rainfall (mm/day) in the GPCPv2.2 and CMAP datasets and for the period 1979–2014.

in the west equatorial Pacific zonal SST gradient and equatorial Walker cells [Hoell and Funk, 2013, 2014]. The combination of the warming trend of SSTs in the Pacific warm pool region and a recent shift of PDV to its cold phase might be expected to lead to a recent increase in the zonal SST gradient in the equatorial Pacific. Figure 16.9 displays anomalous values (1977–1998 base period) of the difference between MAM SSTs averaged over the Pacific warm pool and Niño4 regions in the Pacific based on the HADISST [Rayner et al., 2003] dataset (the trend

in the warm pool is lower in the ERSST data). (The warm pool region is defined as 10°S–10°N, 110°E–150°E, and Niño4 as 5°S–5°N, 160°E–150°W.) There is considerable interannual variability in this series, much associated with the El Niño Southern Oscillation [Hoell and Funk, 2013; Hoell et al., 2014]. There is also an upward shift in 1999, which is identified as the most likely year of a change point ($p < 0.03$) with the timing again consistent with the shift of PDV to its cold phase. During earlier PDV cold phases (not shown), such jumps in the gradient are not as

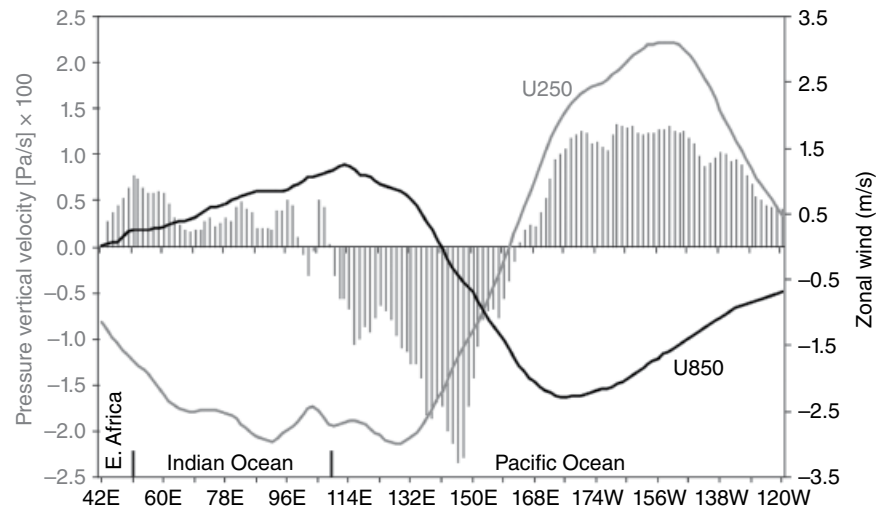


Figure 16.8 Vertical bars indicate the difference in ERA-interim pressure vertical velocity at 500 hPa ($\text{Pa/s} \times 100$) between the periods 1999–2013 and 1979–1998 averaged from 10°S – 10°N . Lines show similar differences in the zonal wind component (m/s) at 850 and 250 hPa.

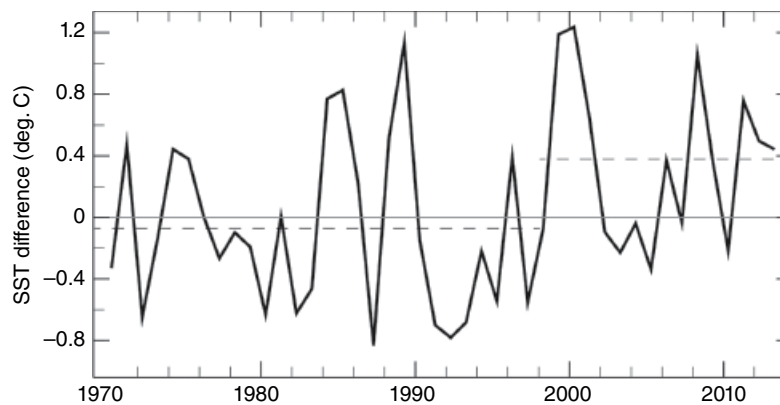


Figure 16.9 Anomalous values (deg. C) of the difference in area average SST between the Pacific warm pool and Niño4 regions during MAM 1970–2013. The dashed horizontal lines show the mean anomaly values for the periods prior to and after a change point in 1999.

readily observed. Issues of SST data quality going back 100 years aside, this suggests the greater influence of the west Pacific warming trend on the gradient in recent years. Again, however, while this could potentially increase the intensity of the rainfall response in the warm pool region in recent years, it does not account for the abrupt shift in behavior in 1998–1999.

In related work, a recent study by *Bayr et al.* [2014] has shown that an upward trend in the strength of Walker circulation (including over the Indian Ocean) since 1979 in the ERA-Interim Reanalysis is predominantly associated with a shift toward more La Niña-like conditions since 1998. This would also appear to be generally consistent with the study by *Jo et al.* [2014] who identify a statistically significant ($p < 0.05$) upward shift in SST in 1998–1999 in the north equatorial current bifurcation

region (8°N – 18°N , 125°E – 160°E) during DJF along with an abrupt upward shift in northward ocean heat transport (0–200 m) in the western Pacific at that time. They hypothesize that the more frequent occurrence of La Niña events in the post-1998 period played a role in maintaining the anomalously warm west Pacific SSTs. Other studies [e.g., *Hoell and Funk*, 2013; *Chen et al.*, 2008] have quantified the tendency for the western equatorial Pacific to warm during La Niña events. *Hoell and Funk* [2013] and *Hoell et al.* [2014] note that the recent warming in this region, while having a contribution from La Niña, also contains a contribution from a long-term upward trend (see Chapter 4).

Taken together, current evidence suggests that while long-term warming of SSTs in the tropical west Pacific, while possibly interacting with PDV to enhance the

Indian Ocean Walker cell in recent years, cannot account for abrupt changes in multiple fields that are observed in 1998–1999, including the regional rainfall decline in East Africa. That the near-global MAM rainfall anomaly pattern in the GPCC data for 1914–1925 is very similar ($p < 0.01$) to that in 1999–2010 strongly suggests PDV alone is capable of generating multiyear droughts, although the *intensity* of recent droughts appears to be greater than past decadal periods (GPCC data quality issues aside). The extent to which anthropogenic climate change may have contributed to the severity of the recent droughts is a fundamentally important question and is an area of active research.

As the attribution of natural versus anthropogenic forcing on East African droughts will necessitate the use of climate model experiments, the final section of this chapter briefly describes the ability of climate models to capture the recent drying in East Africa, linking it to SST anomalies primarily in the tropical Pacific. Some fundamental errors in CMIP5 model simulations of the current climate will also be briefly presented, along with their implications for climate projections.

16.5. CLIMATE MODEL SIMULATIONS OF EAST AFRICAN CLIMATE

16.5.1. AMIP Simulations and the Recent Drying

That the recent drying in East Africa is indeed related to SST variations has been confirmed in several modeling experiments. Some results summarizing these experiments are shown in Figure 16.10, which are all examples of running the atmospheric component of a climate model with forcing primarily from specified SST (so-called AMIP runs). Figure 16.10a shows the difference in MAM rainfall between ensemble mean (30 member) averages for the periods 1999–2013 and 1979–1998 in the ECHAM4.5 model forced with observed, global SSTs (GOGA). Drying is seen over East Africa, with a large-scale anomaly pattern generally quite similar to Figure 16.6a (over land) in observations. Figure 16.10b shows similar results for the same model but when observed SSTs are only specified in the tropical Pacific, with climatological values specified elsewhere. Drying in East Africa again appears, indicating the fundamental role of the tropical Pacific in its forcing. Rainfall anomalies in other regions are again similar to observations and the GOGA runs. Figure 16.10c is the same calculation, but based on an ensemble average of 16 runs from the ECHAM5 model where SSTs have been detrended and set to 1880 equivalent values, as have greenhouse gas concentrations. (These runs were obtained from the Earth Systems Research Laboratory [ESRL] website <http://www.esrl.noaa.gov/psd/repository/alias/facts>.)

Drying over East Africa is again reproduced, along with a similar large-scale anomaly pattern. This latter result suggests that long-term trends in SST are not a necessary condition to generate the recent drying in East Africa (at least in ECHAM5). This would seem consistent with the observational analysis showing earlier decades with drought in East Africa. However, the “residual” SST anomaly field identified after removing the long-term trend is sensitive to the specific methodology used (an example is given in section 16.5.2). As such, additional modeling studies are necessary to more rigorously examine the sensitivity of the model response to various SST anomaly patterns with and without the influence of anthropogenic forcing. This response also needs to be evaluated in more than one model. Figure 16.11, for example, shows the multimodel mean rainfall response (seven models) to observed global SSTs in the Pacific warm pool region. (These model runs are the same as those described in *Seager et al.* [2015].) Consistent with Figure 16.8 for observations, the multimodel mean also generates an abrupt increase in MAM rainfall over the warm pool in 1999, identified as the most likely year of a change point ($p < 0.05$).

16.5.2. CMIP Simulations

Here we very briefly describe a few important issues regarding the ability of CMIP5 models to simulate the current climate of East Africa, with implications for projections. Recent studies by *Yang et al.* [2014, 2015] have shown that the CMIP5 model simulations tend to reverse the relative magnitudes of the short (OND) and long (MAM) rains in East Africa, making the former too wet and the latter too dry climatologically. As shown in Figure 16.12, this appears related to a general bias in the CMIP5 model SST field, particularly over the Indian Ocean. The multimodel mean of simulations from 39 models (see *IPCC* [2013] for their description) generates a larger zonal gradient in equatorial *Indian Ocean* SSTs than is observed during OND (SSTs are too high in the west relative to the east), with the opposite tendency occurring in MAM. (These runs were obtained from the KNMI Climate Explorer at <http://climexp.knmi.nl> using all available ensemble members. Results were unaffected when using a single ensemble member per model [results not shown].)

There is also a 1 month delay in peak positive values of the gradient in CMIP5 relative to observations (April in observations, May in CMIP5). The models also lack virtually any cooling of the western Indian Ocean during the South Asian summer monsoon relative to observations, likely contributing to warmer conditions in OND there compared to observations. The model projections of SST for 2070–2099 (black bars in Fig. 16.12) tend to enhance

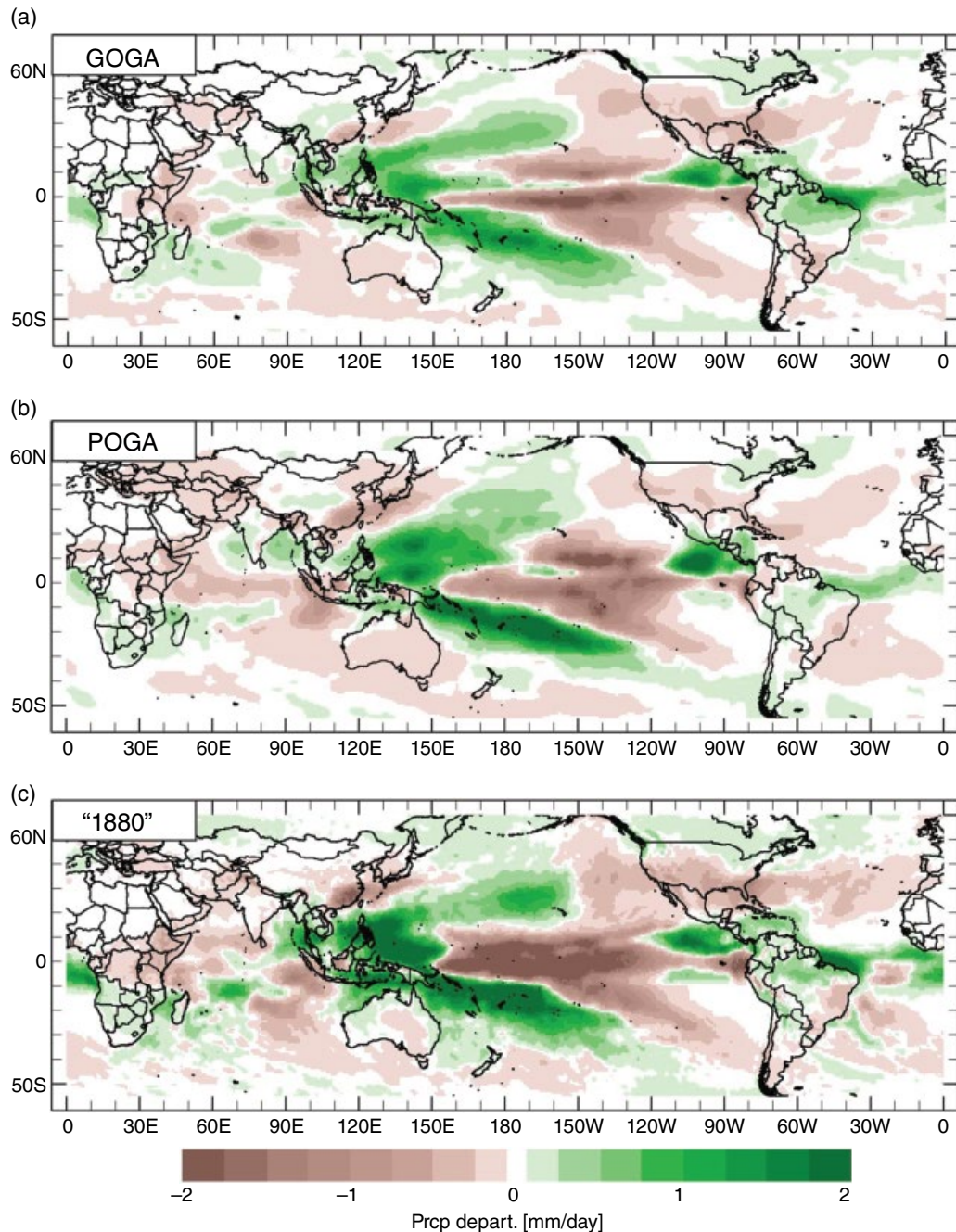


Figure 16.10 (a) Ensemble average MAM precipitation differences (mm/day) between 1999–2012 and 1979–1998 for runs of the ECHAM4.5 model forced with observed global SST. (b) As in (a) but with the observed SSTs limited to the tropical Pacific (120°E–80°W, 25°S–25°N). (c) As in (a) but for the ECHAM5 model forced with detrended SSTs and greenhouse gases fixed at 1880 levels.

these biases in the future and are consistent with wetter projected short and long rains [Yang *et al.*, 2015]. These results alone shed doubt on the reliability of climate projections for East Africa.

Of course, the tropical Pacific also has an important role to play in East African climate. Figure 16.13 provides some comparisons of CMIP5 simulations and observations

over the period 1970–2014. The top panel first shows time series of the CMIP5 multimodel mean, global average (55°S–55°N) SST anomaly (1979–1998 base period) along with observations (from ERSST). Until the late 1990s, the warming trend in the models closely matched observations, followed by a recent warming hiatus in observations since around 2000 (it is not expected that the uninitialized

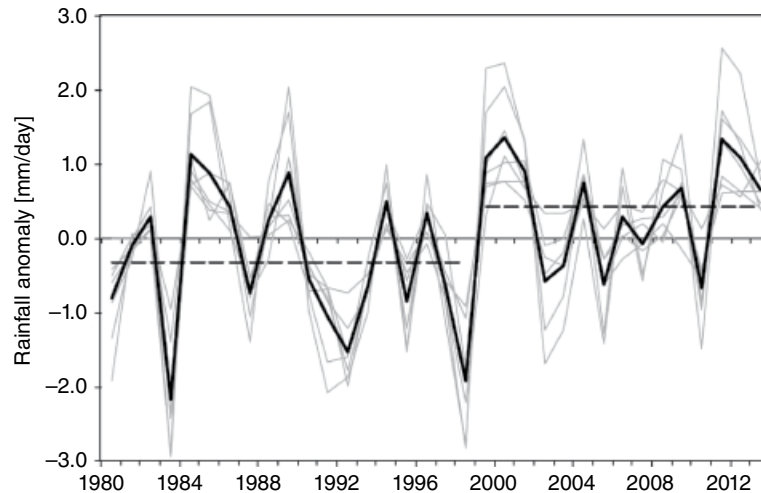


Figure 16.11 Ensemble mean values of anomalous Pacific warm pool precipitation (mm/day, grey lines) obtained from 7 AMIP style climate model simulations forced with observed global SST. Solid black line is the multimodel mean and the dashed horizontal lines indicate mean values for the pre- and post-1999 periods.

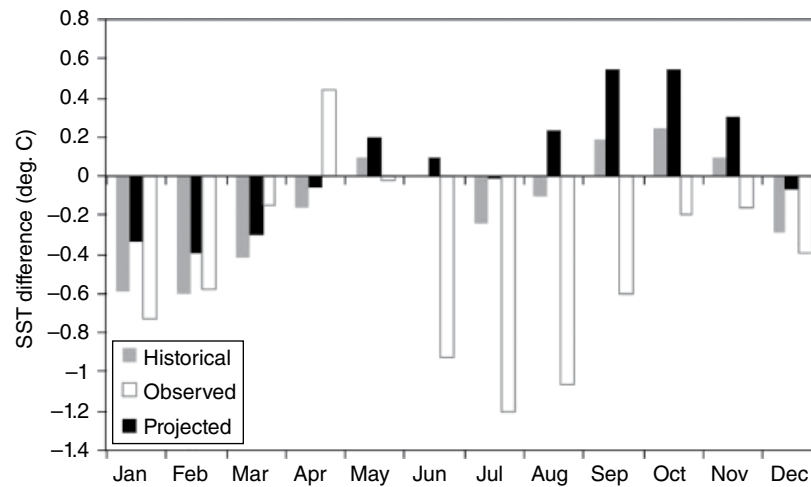


Figure 16.12 Monthly differences in Indian Ocean SST (deg. C) between averages over the western (50°E – 70°E , 10°S – 10°N) and eastern (90°E – 110°E , 10°S – 0°N) portions of the basin. White (grey) bars are climatological averages for the period 1971–2000 in observations (multimodel mean CMIP5 simulations). Black bars indicate the CMIP5 multimodel average values in projections (RCP8.5 scenario) for 2070–2099.

CMIP5 multimodel mean would capture PDV). Figure 16.13b shows a similar plot but for the Niño3.4 region in the east-central Pacific. While observations show no trend over the past four decades, the CMIP5 models show consistent warming over this period, a well-known tendency in the models even before the recent PDV shift [e.g., *Fyfe and Gillett*, 2014]. Whether the eastern Pacific will indeed begin to warm at a faster rate in the future has implications for climate changes in many regions of the world, including East Africa.

Does the observed lack of warming in the eastern Pacific relative to CMIP5 simulations indicate natural climate variations are acting to oppose anthropogenic

warming or are the models simply generating too much warming? Figure 16.13c shows a simple but important example of attempting to quantify the contribution of anthropogenic climate change versus natural variability on SST changes in the west Pacific warm pool region. The figure shows a time series of observed SST anomalies in the region along with two estimates of the residual anomaly obtained after removing the trend. The residual values are computed in two ways: by subtracting the global average, observed SST anomaly (a proxy for the anthropogenic warming signal), and by removing the multimodel mean CMIP5 simulated warm pool anomaly. For the post-1998 period, the magnitude of the residuals

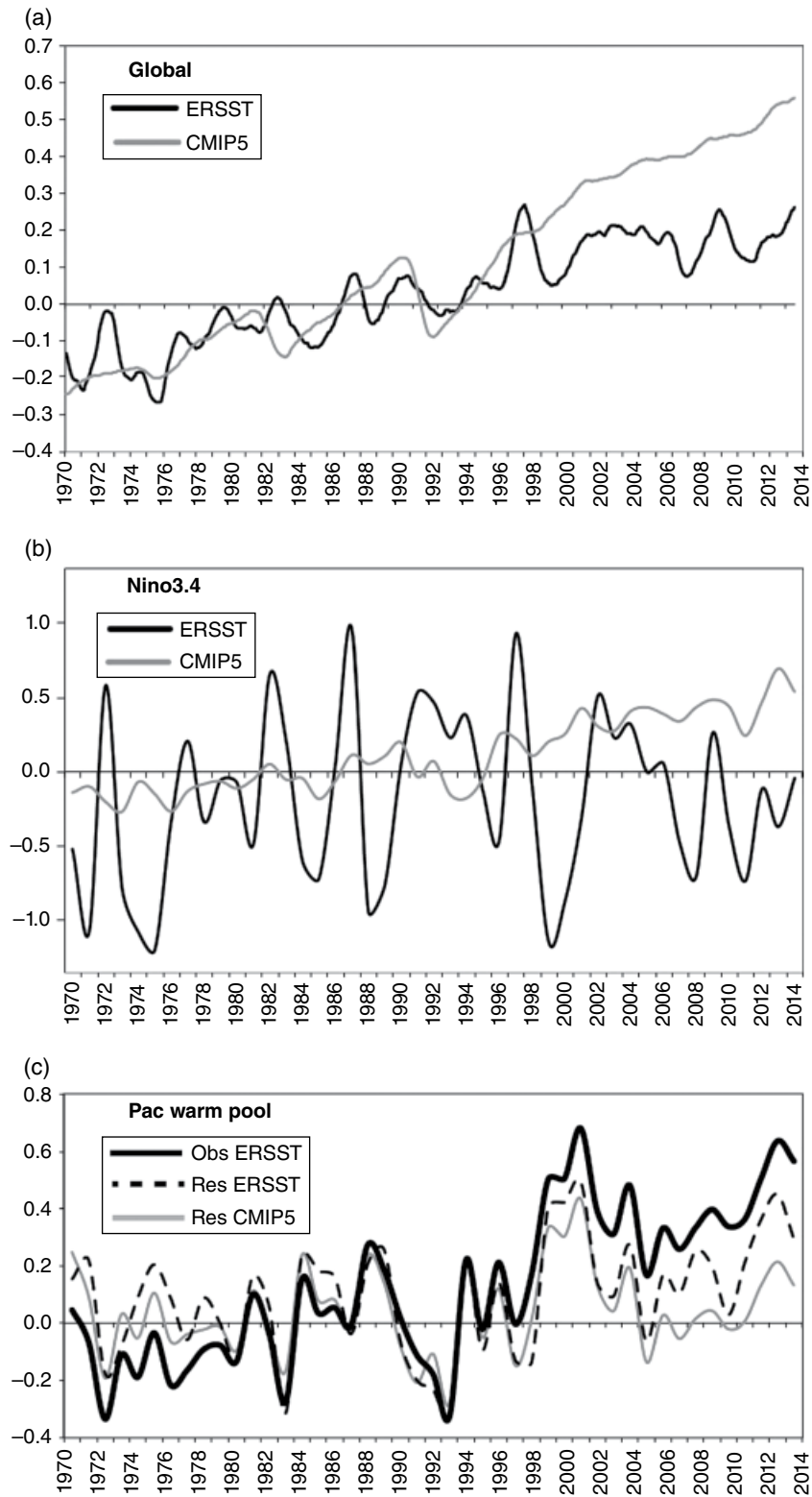


Figure 16.13 (a) Average MAM global (55°S–55°N) SST departure from a 1979–1998 base period mean (deg. C) for observations (black line) and the multimodel mean CMIP5 simulations (grey line). (b) As in (a) but for the Niño3.4 region in the Pacific (120°W–170°W, 5°S–5°N). (c) Observed MAM SST departure from a 1979–1998 base period mean in the Pacific warm pool region (solid black line) and the residual anomalies in this region obtained after removing the time-varying observed global average SST trend (black dashed line) and time-varying CMIP5 multimodel average warm pool trend (grey line).

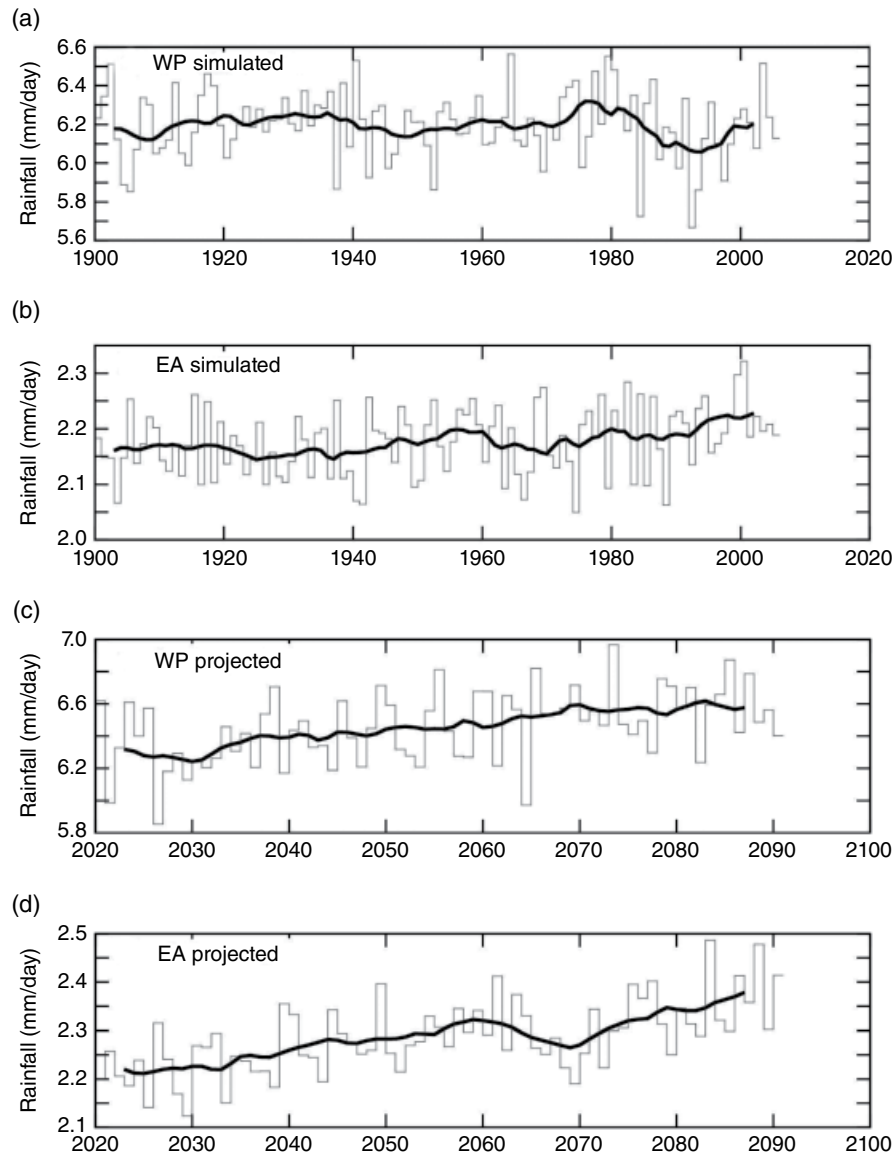


Figure 16.14 (a) Multimodel mean CMIP5 simulations of warm pool rainfall (mm/day) for MAM 1900–2005, with the solid black line representing the 10 year moving average. (b) As in (a) but for East African rainfall (land areas only). (c) and (d) as in (a) and (b) but for model projections (RCP8.5 scenario).

can differ substantially between methods, with the models showing a greater rate of SST increase in the warm pool than is observed in the observed global average value. Which residual estimate is a better representation of natural variations? Are the CMIP5 models realistically capturing the warming of the west Pacific while simultaneously overdoing the warming in the eastern part of the basin or is the former a fortuitous result? There is not a simple answer.

Finally, Figure 16.14 shows time series of the multimodel average CMIP5 simulated MAM rainfall for East Africa and the Pacific warm pool, 1901–2005. While the warm pool region has been warming at a rate generally

consistent with observations (not shown), modeled precipitation for the region exhibits little trend over the past century (Fig. 16.14a) while simulated rainfall in East Africa (Fig. 16.14b) shows a slight increasing trend. The multimodel average projected rainfall for both regions (Fig. 16.14c, d) based on the RCP8.5 scenario shows increasing trends in both locations. In recent observations, the increase in rainfall in the Pacific warm pool region is associated with an enhanced Walker circulation over the Indian Ocean with associated subsidence over East Africa. This indicates that in the models, future changes in SST (and rainfall) in ocean locations outside the west Pacific are clearly important to the rainfall response in East

Africa. Bayr *et al.* [2014] show, for example, an eastward shift of the Pacific Walker cell in CMIP5 projections, generally favoring increased East African rainfall. Thus, while advances are being made in understanding the recent drying in East Africa, what future rainfall changes will be in response to increasing greenhouse gases remains uncertain.

16.6. CONCLUSIONS

What can be concluded about the East African climate paradox? It is argued that several pieces of observational evidence, with support from modeling studies, suggest the recent drying trend was dominated by an abrupt decline around 1998–1999 and associated with a shift of PDV to its cold phase. A long-term warming trend in the tropical Pacific warm pool region may possibly have acted to increase the severity of recent droughts but the timing of the rainfall decline is closely tied to PDV. Further modeling studies are required to investigate the influence of SST warming trends on the severity of recent East African droughts. From the perspective of recent climate behavior, the apparent paradox may be viewed as resulting from a mismatch of timescales, between decadal scale variability (possibly augmented by anthropogenic climate change) and distinct, longer-term climate changes in East Africa arising from increasing greenhouse gases, if the CMIP5 models are taken at face value. In the short term, the expectation is for PDV to retreat from its cold phase and thus a recovery of the long rains from their recent decline.

In the longer term, the impact of increasing greenhouse gases on the climate of East Africa is much less certain. Confidence that the future climate of East Africa will indeed become wetter is currently low. The CMIP5 coupled climate models exhibit significant errors in simulating key aspects of the current climate, not just in East Africa, but also in SST changes in the global oceans. The failure of the models to capture major features of the observed annual cycle of SSTs in the Indian Ocean is particularly problematic. Also critical is whether or not SSTs in the western equatorial Pacific will continue to increase faster than in the central Pacific in response to increasing anthropogenic forcing. If the observed asymmetric warming trends continue, the implication is they will enhance the future likelihood of drought in East Africa, particularly when the eastern portion of the basin cools in association with La Niña (and the cool phase of PDV). If the eastern Pacific in fact warms, the relative likelihood of drought will decrease. Overall, the current climate paradox in East Africa may also result from taking the model projections at face value. Whether or not the future climate in the region will indeed become wetter is considered very much an open question.

ACKNOWLEDGMENTS

This work was supported by grants from the National Science Foundation (award AGS 12-52301) and the National Aeronautical and Space Administration (award NNX12AR39G), which are gratefully acknowledged. Data used in the study were primarily accessed via the IRI Data Library (<http://iridl.ldeo.columbia.edu/>), with data for Figure 16.14 obtained from the Royal Netherlands Meteorological Institute (KNMI) Climate Explorer (https://climexp.knmi.nl/selectfield_cmip5.cgi).

REFERENCES

- Bayr, T., D. Dommenges, T. Martin, and S. B. Power (2014), The eastward shift of the Walker Circulation in response to global warming and its relationship to ENSO variability, *Climate Dyn.*, *43*, 2747–2763; doi:10.1007/s00382-014-2091-y.
- Camberlin, P., and R. E. Okoola (2003), The onset and cessation of the “long rains” in eastern Africa and their interannual variability, *Theor. App. Climatol.*, *75*, 43–54; doi:10.1007/s00704-002-0721-5.
- Camberlin, P., B. Fontaine, S. Louvet, P. Oettli, and P. Valimba (2010), Climate adjustments over Africa accompanying the Indian monsoon onset, *J. Climate*, *23*, 2047–2064; doi:10.1175/2009JCLI3302.1.
- Cecchi, F., and W. C. Robinson (2013), Mortality among populations of southern and central Somalia affected by severe food insecurity and famine during 2010–2012, *FAO and FEWS NET*; <http://www.fsnao.org/in-focus/study-report-mortality-among-populations-southern-and-central-somalia-affected-severe-food->.
- Chen, J., A. D. Del Genio, B. E. Carlson, and M. G. Bosilovich (2008), The spatiotemporal structure of twentieth-century climate variations in observations and reanalyses, Part II: Pacific pan-decadal variability, *J. Climate*, *21*, 2634–2650.
- Christensen, J. H., and coauthors (2007), Regional climate projections, in *Climate Change 2007: The Physical Science Basis*, edited by S. Solomon et al., Cambridge University Press, 866–872.
- Dee, D. P., and coauthors (2011), The ERA-interim reanalysis: Configuration and performance of the data assimilation system, *Quart. J. Roy. Meteor. Soc.*, *137*, 553–597; doi: 10.1002/qj.828.
- FAO, IFAD, and WFP (2014), The State of Food Insecurity in the World 2014, Strengthening the enabling environment for food security and nutrition, Rome, FAO.
- FEWS NET (2011), Past year one of the driest on record in the eastern Horn, *Famine Early Warning System Network Report*, June 14, 2011, U.S. Agency for International Development, Washington, DC.
- Funk, C., G. Husak, J. Michaelsen, S. Shukla, A. Hoell, B. Lyon, M. P. Hoerling, B. Liebmann, T. Zhang, J. Verdin, G. Galu, G. Eilerts, and J. Rowland (2013), Attribution of 2013 and 2003–2012 rainfall deficits in eastern Kenya and southern Somalia, in *Explaining Extreme Events of 2012 from a Climate Perspective*, *Bull. Amer. Meteor. Soc.*, *94*, S1–74.

- Funk, C. C., P. J. Peterson, M. F. Landsfeld, D. H. Pedreros, J. P. Verdin, J. D. Rowland, B. E. Romero, G. J. Husak, J. C. Michaelsen, and A. P. Verdin, (2014), *A Quasi-Global Precipitation Time Series for Drought Monitoring*, U.S. Geological Survey Data Series 832; <http://dx.doi.org/10.3133/ds832>.
- Fyfe, J. C., and N. P. Gillett (2014), Recent observed and simulated warming, *Nature Climate Change*, *4*, 150–151.
- Hoell, A., and C. Funk (2013), The ENSO-related West Pacific sea surface temperature gradient, *J. Climate*, *26*, 9545–9562.
- Hoell, A., and C. Funk (2014), Indo-Pacific sea surface temperature influences on failed consecutive rainy seasons over eastern Africa, *Climate Dyn.*, *43*, 1645–1660; doi:10.1007/s00382-013-1991-6.
- Hoell, A., C. Funk, and M. Barlow (2014), La Niña diversity and northwest Indian Ocean rim teleconnections, *Climate Dyn.*, *43*, 2707–2724.
- Huffman, G. J., R. F. Adler, D. T. Bolvin, and G. Gu (2009), Improving the global precipitation record: GPCP version 2.1, *Geophys. Res. Lett.*, *36*, L17808; doi:10.1029/2009GL040000.
- IPCC (2013), Annex I: Atlas of Global and Regional Climate Projections, edited by G. J., van Oldenborgh, M. Collins, J. Arblaster, J. H. Christensen, J. Marotzke, S. B. Power, M. Rummukainen, and T. Zhou, in *Climate Change 2013: The Physical Science Basis, Contribution of Working Group I to the Fifth Assessment Report of the Intergovernmental Panel on Climate Change*, edited by T. F. Stocker, D. Qin, G.-K. Plattner, M. Tignor, S. K. Allen, J. Boschung, A. Nauels, Y. Xia, V. Bex, and P. M. Midgley, Cambridge University Press, Cambridge, UK and New York, USA.
- Jo, H.-S., S.-W. Yeh, and B. P. Kirtman (2014), Role of the western tropical Pacific in the North Pacific regime shift in the winter of 1998–1999, *J. Geophys. Res. Oceans*, *119*, 6161–6170; doi:10.1002/2013JC009527.
- Kajikawa, Y., T. Yasunari, S. Yoshida, and H. Fujinami (2012), Advanced Asian summer monsoon onset in recent decades, *Geophys. Res. Lett.*, *39*, L03803; doi:10.1029/2011GL050540.
- Liebmann, B., M. P. Hoerling, C. Funk, I. Bladé, R. M. Dole, D. Allured, X. Quan, P. Pegion, J. K. Eischeid (2014), Understanding recent eastern Horn of Africa rainfall variability and change, *J. Climate*, *27*, 8630–8645.
- Liebmann, B., R. M. Dole, C. Jones, I. Bladé, and D. Allured (2010), Influence of choice of time period on global surface temperature trend estimates, *Bull. Amer. Meteor. Soc.*, *91*, 1485–1491; doi:10.1175/2010BAMS3030.1.
- Lyon, B (2014), Seasonal drought in the Greater Horn of Africa and its recent increase during the March-May long rains, *J. Climate*, *27*, 7953–7975.
- Lyon, B., and D. G. DeWitt (2012), A recent and abrupt decline in the East African long rains, *Geophys. Res. Lett.*, *39*, L02702; doi:10.1029/2011GL050337.
- Lyon, B., A. G. Barnston, and D. G. DeWitt (2014), Tropical Pacific forcing of a 1998–99 climate shift: Observational analysis and climate model results for the boreal spring season, *Climate Dyn.*, *43*, 893–909; doi:10.1007/s00382-013-1891-9.
- Mantua, N. J., S. R. Hare, Y. Zhang, J. M. Wallace, and R. C. Francis (1997), A Pacific interdecadal climate oscillation with impacts on salmon production, *Bull. Amer. Meteor. Soc.*, *78*, 1069–1079.
- Rayner, N. A., D. E. Parker, E. B. Horton, C. K. Folland, L. V. Alexander, D. P. Rowell, E. C. Kent, and A. Kaplan (2003), Global analyses of sea surface temperature, sea ice, and night marine air temperature since the late nineteenth century, *J. Geophys. Res.*, *108*, 4407; doi:10.1029/2002JD002670.
- Schneider, U., T. Fuchs, A. Meyer-Christoffer, and B. Rudolf (2008), *Global Precipitation Analysis Products of the GPCP*, Global Precipitation Climatology Centre (GPCC), DWD, Internet Publication, 1–12; http://www.ccc.org/Atlas/Files/Precipitation/GPCC_intro_products_2008.pdf.
- Seager, R., M. Hoerling, S. Schubert, H. Wang, B. Lyon, A. Kumar, J. Nakamura, and N. Henderson (2015), Causes of the 2011 to 2014 California drought, *J. Climate*, *28*, 6997–7024.
- Shongwe, M. E., G. J. van Oldenborgh, B. van den Hurk, and M. van Aalst (2011), Projected changes in mean and extreme precipitation in Africa under global warming, Part II: East Africa, *J. Climate*, *24*, 3718–3733; doi:10.1175/2010JCLI2883.1.
- UN OCHA (2011), *Eastern Africa Drought, Humanitarian Rep. 4*, United Nations Organization for the Coordination of Humanitarian Affairs; http://reliefweb.int/sites/reliefweb.int/files/resources/Full_Report_1717.pdf.
- Van den Dool, H. M., and R. M. Chervin (1986), A comparison of month-to-month persistence of anomalies in a general circulation model and in the earth's atmosphere, *J. Atmos. Sci.*, *43*, 1454–1466.
- Wang, X. L. (2008), Accounting for autocorrelation in detecting mean-shifts in climate data series using the penalized maximal t or F test, *J. Appl. Meteor. Clim.*, *47*, 2423–2444.
- Xie, P., and P. A. Arkin (1997), Global precipitation: A 17-year monthly analysis based on gauge observations, satellite estimates and numerical model outputs, *Bull. Amer. Meteor. Soc.*, *78*, 2539–2558.
- Yang, W., R. Seager, M. A. Cane, and B. Lyon (2014), The East African long rains in observations and models, *J. Climate*, *27*, 7185–7202.
- Yang, W., R. Seager, M. A. Cane, and B. Lyon (2015), The annual cycle of East African precipitation, *J. Climate*, *28*, 2385–2404.